Progress In Electromagnetics Research B, Vol. 95, 23–40, 2022

Detection of Inter-Turn Short-Circuit on a Doubly Fed Induction Machine with D-Q Axis Representation — Application to Different Power Levels

Habachi Bilal[1], Eric J. R. Sambatra[2], Nicolas Heraud[1, *], Jean-Marie Razafimahenina[3], and Svetlana Dyagileva[1]

Abstract—This paper presents a method based on the elliptical representation of D-Q currents to detect and quantify an Inter-Turn Short-Circuit (ITSC) fault in windings of a Doubly Fed Induction Machine (DFIM). ITSC is said to be an evolving fault, so it is essential to detect it at an early stage to avoid damage on the machine. Therefore, the method should be able, on the first hand, to detect the defect and, on the second hand, to quantify its severity. Moreover, this study requires less computation time than classical methods such as harmonic analysis. In this paper, current data are acquired at a sampling frequency of 1 kHz. This method is successful with this low data sampling rate. In order to validate this study, a theoretical analysis with two models of different DFIM powers (0.3 kW, 0.25 kW and 11 kW) is carried out (healthy case and faulty case: presence of ITSC), and these results are confirmed by using platforms including Doubly Fed Induction Machines (DFIMs) and Data Acquisition (DAQ) system.

1. INTRODUCTION

In electrical power production systems and industrial processes, DFIMs have a very important role. To avoid costly downtime and breakdowns, early detection of faults is vital. Stator, rotor, and bearings are the three main components of an induction machine affected more by the various anomalies. According to the studies [1,2], in squirrel cage induction motors, bearing and stator winding related failures account for the largest percentage of total failures. More recent studies dealing with the distribution of faults in induction machines show that the shaft or coupling (3%), rotor (7%), stator windings (21%), and bearings (69%) are the most failed components [3, 4].

Inter-Turn Short-Circuit (ITSC) fault is a common electrical fault in induction machines, and generally, they are caused by insulation failures, mechanical stresses, thermal stresses, and partial discharges [5, 6]. If these defects are unresolved, they lead to increased operating costs due to machine downtime, hence the need for effective reliability monitoring and noninvasive fault diagnosis methods to reduce unplanned downtime and associated high costs [5]. Therefore, it is essential to propose methods to detect ITSC anomalies at early stage when machine is running. Many works on detecting this type of fault can be found in [7–12]. In [7], the authors propose a Luenberger observer to detect the inter turn short-circuit and locate the phase where it appears. Abdelmadjid et al. present a Fault Tolerant Control (FTC) in the presence of a fault on a stator (25 short-circuited turns), but the inter short circuit is not quantified [8]. In [9], Kato et al. describe a method to detect fault in stator winding of an induction motor by the direct detection of its negative sequence current as the works proposed by Im and

Received 12 January 2022, Accepted 22 March 2022, Scheduled 5 April 2022
* Corresponding author: Nicolas Heraud (heraud@univ-corse.fr).
[1] UMR CNRS 6134, Department of Renewable Energies, University of Corsica, Corte 20250, France. [2] Department of Industrial Engineering, Higher Institute of Techonology, BP 509, Antsiranana 201, Madagascar. [3] Laboratory of Industrial Electronics, Department of Electrical Engineering, University of North Madagascar, Antsiranana 201, Madagascar.

Gu [10]. In their works, Roshanfekr and Jalilian present a Magnetic Equivalent Circuit model (MEC) to simulate short-circuited turn [11]. An analytical and experimental study to detect short-circuited turns through a frequency analysis is proposed by Razafimahefa et al. [12], and these authors propose Park Vector Approach (AVP) [13]. Wang et al. [14] describe a short-circuit model with a resistor and a quantification of ITSC by an analysis of specific harmonics of short-circuit current. The most crucial disadvantage of the proposed method is the measurement of this current in real conditions because it is impossible to access it, excepted on an experimental platform. In work [15], Pires et al. use unbalance of stator voltage and stator current. So, they construct Volterra series to detect ITSC. The results presented seem interesting but need heavy calculation. In other works [16], Foito et al. focus on Park transform technique of mass center of the stator current. Then in the D-Q basis, they manage to obtain a specific model of the engine subjected to ITSC by selecting the center of mass and the radius of the circumference which depends on ITSC severity. On the other hand, this technique does not specify the phase where ITSC is localized.

In this paper, a noninvasive method by using the Park transform is proposed. The currents on the three phases can be reduced to D-Q basis of two dimensions. From this representation, it is possible to detect and quantify ITSC. The first part of this article describes DFIM models in healthy operation and faulty operation (in presence of ITSC). Two models are compared with experimental platform measurements. The second part is devoted to ITSC detection and quantification. The last part consists of detecting and quantifying the ITSC under different conditions (2.5%, 5%, 10%, 20%, 30%, and 40% of ITSC). Theoretical (DFIM powers of 0.3 kW, 0.25 kW, and 11 kW) and practical (DFIM powers of 0.3 kW and 0.25 kW) results are presented through these different stages.

2. THEORETICAL STUDIES

2.1. Healthy Condition

The differential system in Eqs. (1) to (4), modeling the induction machine, can be written in a vector-matrix form such as [12]:

$$[V] = [R][I] + [I]\omega\frac{d[L]}{d\theta} + [L]\frac{d[I]}{dt} \tag{1}$$

$[V]$ is the vector of the stator and rotor voltages; $[I]$ is the vector of the stator and rotor currents; $[R]$ is the matrix of stator and rotor resistances; $[L]$ is the matrix of the stator and the rotor inductances and ω the shaft rotational speed. The equation of motion is as follows:

$$J\frac{d\omega}{dt} + f_v\omega = T_e - T_l \tag{2}$$

$$\omega = \frac{d\theta}{dt} \tag{3}$$

$$T_e = \frac{1}{2}[I]^T\frac{d[L]}{d\theta}[I] \tag{4}$$

J is the moment of total inertia of the rotor, f_v the viscous friction torque, T_e the electromagnetic torque, T_l the load torque, and θ the angular position.

2.2. DFIM Analytical Model with ITSC

In this paper, the ITSC fault model, which will be used, is based on the one proposed by the works of [7]. This model can quantitatively describe ITSC fault at any level and in any single phase. It introduces f_x model parameter to describe the fault position in the DFIM stator [7]. The advantage by using this model is to simulate healthy and faulty conditions. In this paper, the fault position parameter f_x is defined as follows: the fault occurs in the A phase of the DFIM stator. In the following equations, the capital letters (A, B, and C) indicate that the component is located on the stator phase. The small letters (a, b, and c) show that the constituent is situated on the rotor phase. The model of the machine takes into account the classical assumptions [12, 13]. The default position parameter f_x is defined by:

$f_x = f_A = [1\ 0\ 0]^T$. The indices s and r designate stator and rotor. The variables containing f are associated with the short-circuited turns.

$$n_f = \frac{N_f}{N_s} \tag{5}$$

N_f is the number of turns short-circuit. N_s is the number of turns in a phase.

The voltage and flux model equations in the two DFIM windings are given as follows:

$$\begin{bmatrix} V_{ABC} \\ V_{abc} \\ V_f \end{bmatrix} = \begin{bmatrix} R_s & 0_{3\times3} & -n_f R_s f_x \\ 0_{3\times3} & R_r & 0_{3\times1} \\ n_f R_s f_x^T & 0_{1\times3} & -\|n_f R_s f_x\| \end{bmatrix} \begin{bmatrix} I_{ABC} \\ I_{abc} \\ I_f \end{bmatrix} + \frac{d}{dt} \begin{bmatrix} \lambda_{ABC} \\ \lambda_{abc} \\ \lambda_f \end{bmatrix} \tag{6}$$

$$\begin{bmatrix} \lambda_{ABC} \\ \lambda_{abc} \\ \lambda_f \end{bmatrix} = \begin{bmatrix} L_{ss} & L_{sr} & -n_f L_{ss} f_x \\ L_{rs} & L_{rr} & -n_f L_{rs} f_x \\ n_f L_{ss} f_x^T & n_f L_{sr} f_x^T & -n_f L_f \end{bmatrix} \begin{bmatrix} I_{ABC} \\ I_{abc} \\ I_f \end{bmatrix} \tag{7}$$

The resistances and self inductances matrices are given as follows:

$$R_s = \begin{bmatrix} r_s & 0 & 0 \\ 0 & r_s & 0 \\ 0 & 0 & r_s \end{bmatrix}, \quad R_r = \begin{bmatrix} r_r & 0 & 0 \\ 0 & r_r & 0 \\ 0 & 0 & r_r \end{bmatrix}$$

$$L_{ss} = \begin{bmatrix} L_s & M_s & M_s \\ M_s & L_s & M_s \\ M_s & M_s & L_s \end{bmatrix}, \quad L_{rr} = \begin{bmatrix} L_r & M_r & M_r \\ M_r & L_r & M_r \\ M_r & M_r & L_r \end{bmatrix}$$

The stator-rotor (L_{sr}) and rotor-stator (L_{rs}) mutual inductances are given by:

$$L_{sr} = M_{sr} \begin{bmatrix} \cos\theta_r & \cos\left(\theta_r + \frac{2\pi}{3}\right) & \cos\left(\theta_r - \frac{2\pi}{3}\right) \\ \cos\left(\theta_r - \frac{2\pi}{3}\right) & \cos\theta_r & \cos\left(\theta_r + \frac{2\pi}{3}\right) \\ \cos\left(\theta_r + \frac{2\pi}{3}\right) & \cos\left(\theta_r - \frac{2\pi}{3}\right) & \cos\theta_r \end{bmatrix}$$

$$L_{rs} = L_{sr}^T$$

The self inductances of the stator and rotor windings including the inter-turn short circuit can be expressed by:

$$L_s = l_{sp} + l_{ls}, \quad L_r = l_{rp} + l_{lr}, \quad L_f = n_f l_{sp} + l_{ls}$$

The stator-stator and rotor-rotor mutual inductances are equal to:

$$M_s = -\frac{1}{2} l_{sp}, \quad M_r = -\frac{1}{2} l_{rp}$$

The electromagnetic torque frame is defined as follows:

$$T_e = p\left({I_{ABC}}^T \frac{\partial L_{sr}}{\partial \theta_r} I_{abc} + n_f f_x^T I_f \frac{\partial L_{sr}}{\partial \theta_r} I_{abc} \right) \tag{8}$$

V_{ABC} and V_{abc} are the voltages on the stator and rotor windings, respectively, and V_f is the voltage due to ITSC. I_{ABC} and I_{abc} are the currents on the stator and rotor windings, respectively, and I_f is the current due to ITSC. λ_{ABC} and λ_{abc} are the fluxes on the stator and rotor, respectively, and λ_f is the flux due to ITSC. R_s and R_r are the resistances on the stator and rotor windings. L_{ss} and L_{rr} are the self inductances on the stator and rotor windings. L_{sr} is the stator-rotor mutual inductances, and L_{rs} is the rotor-stator mutual inductances. L_s and L_r are the self inductances of the stator and rotor. l_{sp} and l_{rp} are the own inductances of the stator and the rotor. l_{ls} and l_{lr} are the leakage inductances of the stator and rotor. L_f is the inductance due to ITSC. M_s is the stator-stator mutual inductances, and M_r is the rotor-rotor mutual inductances. T_e is the electromagnetic torque, and p is the number of pole pairs.

3. EXPERIMENTAL SETUP

3.1. Default Setting

Figure 1 represents a coil of an elementary winding whose input and output are respectively noted as A and X. On this coil there is a short circuit between turns at a1 and a2 contact points.

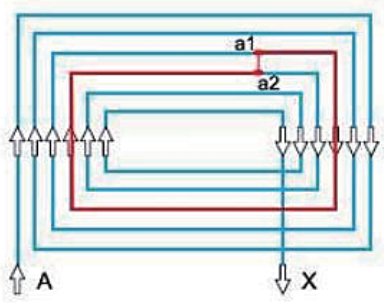

Figure 1. ITSC schema.

3.2. Materials and Methods

The proposed model was used to simulate a DFIM with standard specifications which are presented in Table 1. Each stator phase contains 6 coils in series. Moreover, each coil is made up of 133 turns or 798 series turns. Simulations were performed for the nominal load in healthy and faulty cases. In the faulty case, the different rates of short circuit are presented in Table 2.

Table 1. Characteristics of DFIM1.

Specifications	Values	Units
Rated frequency, f	50	Hz
Rated voltage	230/400	V
Rated power, P_n	0.3	kW
Nominal speed	1488	r/min
Rated current	1.5/0.87	A
Self inductances, l_{sp}, l_{rp}	0.79/0.79	H
Moment of inertia	0.008	kg·m^2
Resistances, r_s, r_r	33/16.5	Ω
Number of pole pairs, p	2	

Simulations were performed for the nominal load in healthy and faulty cases. In the faulty case, there are the different rates of short circuit (Table 2). In this study, the short-circuit fault is located on phase A of the stator winding. In order to validate the model, experimental measurements were carried out from the DFIM1 (see Figure 2) in both cases: healthy and faulty. The sampling frequency of experimental data is $f_s = 1\,\text{kHz}$.

Figure 2 shows the experimental equipment. It consists of an induction machine (DFIM1), current sensors, a data acquisition system (DAQ), and a computer.

The ITSC fault is characterized by a high amplitude of short-circuit current, and it is an evolutionary fault. In theoretical and experimental studies, the hypothesis that the evolution of the defect depends on the resistance R_f is retained. For example, this current is quite high since it is equal to 10 A when the machine is absorbing 1 A. Note that the short circuit current is inversely proportional

Table 2. The different short-circuited turns on phase A of the DFIM1.

Number of short circuit turns N_{sc}	**ITSC rate (%)** n_{sc}
20	2.5
40	5
80	10
160	20
240	30
320	40

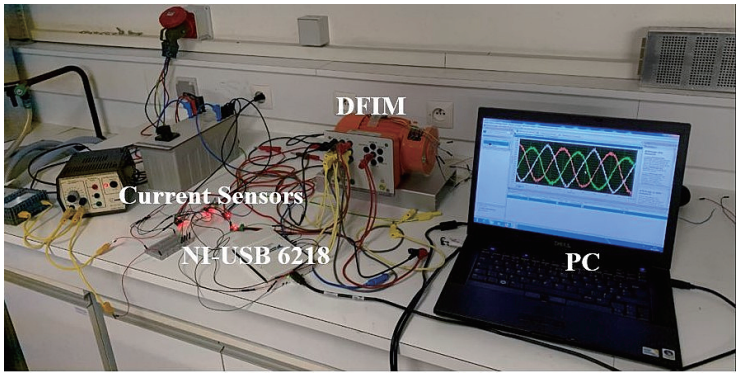

Figure 2. Experimental setup for the winding fault in induction machine.

to the value of short circuit resistance. We propose a stator current analysis with the Park transform to have more precision on the evolution of the ITSC defect.

4. PARK TRANSFORMATION

One way to detect certain anomalies, such as the short circuit fault between turns, is to analyze the harmonics contained in the stator current. This technique is called "Motor Current Signature Analysis (MCSA)", and it is developed in [9, 11, 17] on an induction motor and a doubly fed induction generator (DFIG). In our study, we focus on the geometrical properties of currents and the Park transform [18–21].

$$\begin{cases} i_{sd} = \sqrt{\dfrac{2}{3}} I_A - \dfrac{1}{\sqrt{6}} I_B - \dfrac{1}{\sqrt{6}} I_C \\ i_{sq} = \dfrac{1}{\sqrt{2}} I_B - \dfrac{1}{\sqrt{2}} I_C \end{cases} \tag{9}$$

The Park transform is a proven dimensionally reduced technique for balanced three-phase systems. In fact, it allows to project a three-dimensional space (I_A, I_B, and I_C) to two-dimensional space (i_{sd} and i_{sq}) without any loss of information. The projection of a sinusoidal and symmetrical signal, describes a circle in 2D space. However, when the DFIM1 is subject to a defect, the geometric shape of the current changes to an ellipse with a specific orientation.

The currents are presented in the D-Q basis when the DFIM1 has a ITSC fault (10% and 20%). Figure 3 highlights the methodology. Figure 3 shows the similarity between the theoretical and practical data representations.

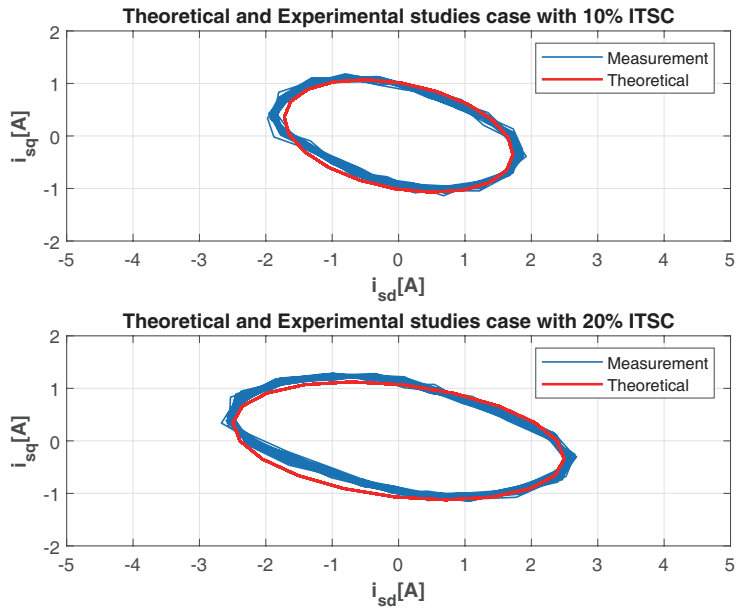

Figure 3. Stator currents in squaring (10% and 20%): measurement and simulation.

4.1. Presentation of Ellipse Coefficients in ITSC Case

As soon as a defect appears, the space (E) of Figure 4 is deformed, and the circle in the healthy case becomes an ellipse characterized by two axes (major axis and minor axis). The size of (E) is quantified by parameters A for the major axis and B for the minor axis which are the direct and quadrature axis currents under the effect of the defect. At the same time, if a defect occurs, both axes rotate, so that the major axis is no longer aligned with D, and the minor axis is no longer confused with Q. This rotation is characterized by the angle Phi.

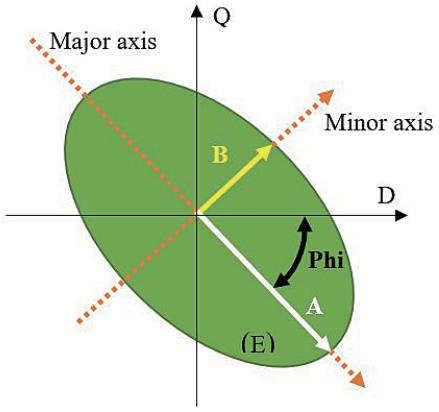

Figure 4. Ellipse parameters A, B and Phi.

Before presenting ellipse coefficients obtained from the model and measurement of DFIM1 currents, it is useful to specify the network harmonic pollution. For that, Table 3 specifies the total harmonic distortion (THD_i) (10) of the two currents in direct quadrature i_{sd} and i_{sq}.

$$\text{THD}_i(\%) = 100 \times \frac{\sqrt{\sum_{h=2}^{\infty} I_h^2}}{I_1} \tag{10}$$

with I_h being the Root Mean Square (RMS) value of the harmonic magnitude corresponding to the h^{th} harmonic order and I_1 the harmonic of rank 1 [22].

Looking at Table 3 above, the THD of i_{sd} reveals a harmonic pollution for 10% and 20% of ITSC in the DFIM1 stator winding. Similarly, the THD of i_{sq} increases according to the ITSC but less significantly than THD of i_{sd}.

Table 3. THD_i of the two currents i_{sd} and i_{sq}.

Park currents	**Healthy**	**10% ITSC**	**20% ITSC**
i_{sd}	4.35	9.82	14.08
i_{sq}	2.50	5.83	7.85

Now the values of the three coefficients (A, B, Phi) obtained from the ellipses of Figure 3 are presented in Table 4 to Table 6. A is the major axis, B the minor axis, and Phi the orientation of the ellipse. With these coefficients, as shown in Table 4 to Table 6, it is possible to easily detect the fault and to quantify the ITSC rate in the windings.

Table 4. Coefficient model A: Theoretical and experimental studies.

ITSC rate (%) n_{sc}	$\mathbf{A_{Experimental}}$	$\mathbf{A_{Theoretical}}$
2.5	1.20	1.19
20	2.57	2.52
30	3.48	3.43
40	4.74	4.66

A, B, and Phi are short circuit rate functions whose coefficients are identified by least squares technique as explain in the paper [22]. The columns 2 and 3 of Table 4 show similar results and indicate the relevance of the approach on both the theoretical and experimental aspects. The representation of data from columns 1 and 2 (respectively 3) forms a straight line in the affine plane and can be modeled by Eq. (11). According to the values given by Table 4, the major axis A can be expressed as:

$$A = p_1 n_{sc} + p_2 \tag{11}$$

with n_{sc} being the inter-turn short-circuit rate (%).

$p_1 = 0.13$ for the experimental and 0.12 for the theoretical studies.

$p_2 = 0.9$ for the experimental and 0.84 for the theoretical studies.

The columns 2 and 3 of Table 5 show similar results and indicate the relevance of the approach. The representation of data from columns 1 and 2 (respectively 3) forms a straight line in the affine plane too and can be modeled by Eq. (12).

Table 5. Coefficient model B: Theoretical and experimental studies.

ITSC rate (%) n_{sc}	$\mathbf{B_{Experimental}}$	$\mathbf{B_{Theoretical}}$
2.5	0.83	0.97
20	0.96	1.04
30	1.01	1.11
40	1.06	1.19

According to the values given by Table 5, the minor axis B can be expressed as:

$$B = p_3 n_{sc} + p_4 \tag{12}$$

$p_3 = 0.006$ for the experimental and 0.006 for the theoretical studies.
$p_4 = 0.82$ for the experimental and 0.94 for the theoretical studies.

The columns 2 and 3 of Table 6 show quite similar results and indicate the relevance of the approach. But these results are less good than the previous tables. Nevertheless, the representation of data from columns 1 and 2 (respectively 3) forms a rational function in the affine plane and can be modeled by Eq. (13).

Table 6. Coefficient model *Phi*: Theoretical and experimental studies.

ITSC rate (%) n_{sc}	**Phi$_{\text{Experimental}}$** (rad)	**Phi$_{\text{Theoretical}}$** (rad)
2.5	0.50	0.59
20	0.24	0.35
30	0.21	0.25
40	0.19	0.17

According to the values given by Table 6, the orientation *Phi* can be expressed as:

$$Phi = \frac{p_5}{(n_{sc} + p_6)} \tag{13}$$

$p_5 = 9.67$ for the experimental and 11.86 for the theoretical studies.
$p_6 = 16.99$ for the experimental and 17.43 for the theoretical studies.

In order to validate the three models presented by above Eqs. (11) to (13), Table 7 shows the three parameters A_{Th1}, B_{Th1}, and Phi_{Th1} for 5% and 10% calculated from Eqs. (11) to (13) and the DFIM1 theoretical data. Next, these values are compared to the results A_{Ex1}, B_{Ex1}, and Phi_{Ex1} obtained from these relationships and DFIM1 experimental data.

Table 7. *A*, *B* and *Phi* obtained from calculations.

ITSC rate (%) n_{sc}	**A$_{\text{Ex1}}$** Experimental for DFIM1	**A$_{\text{Th1}}$** Theoretical for DFIM1
5	1.55	1.44
10	2.22	2.04
ITSC rate (%) n_{sc}	**B$_{\text{Ex1}}$** Experimental for DFIM1	**B$_{\text{Th1}}$** Theoretical for DFIM1
5	0.85	0.97
10	0.88	1
ITSC rate (%) n_{sc}	**Phi$_{\text{Ex1}}$** Experimental for DFIM1	**Phi$_{\text{Th1}}$** Theoretical for DFIM1
5	0.44 rad	0.53 rad
10	0.36 rad	0.43 rad

On the other hand, Table 8 shows the three parameters A_{Th1}, B_{Th1}, and Phi_{Th1} for 5% and 10% obtained directly from the ellipses and the DFIM1 theoretical data and A_{Ex1}, B_{Ex1}, and Phi_{Ex1} obtained directly from the ellipses and DFIM1 experimental data. The calculations give convincing results and are close to the results obtained in Table 7.

Table 8. A, B and Phi obtained from ellipses.

ITSC rate (%) n_{sc}	$\mathbf{A_{Ex1}}$ Experimental for DFIM1	$\mathbf{A_{Th1}}$ Theoretical for DFIM1
5	1.47	1.42
10	1.89	1.84
ITSC rate (%) n_{sc}	$\mathbf{B_{Ex1}}$ Experimental for DFIM1	$\mathbf{B_{Th1}}$ Theoretical for DFIM1
5	0.84	0.99
10	0.89	1.02
ITSC rate (%) n_{sc}	$\mathbf{Phi}_{Ex1}$ Experimental for DFIM1	$\mathbf{Phi_{Th1}}$ Theoretical for DFIM1
5	0.44 rad	0.57 rad
10	0.33 rad	0.49 rad

The presented method shows that the number of short-circuited turns can be deduced with accuracy, and calculations are easy.

In the second part of this work, using the same methodology as previously described, the results of fault detection on another machine (named DFIM2) of the same power level (0.25 kW) as the first machine (DFIM1) are presented. The interest is to ensure that the described method can be easily used on other machines.

5. DFIM2 STUDY

5.1. DFIM2 Experimental Setup

The stator of DFIM2 has 36 slots, and the rotor has 18 slots. Each phase has 6 windings in series, and each winding has 68 turns. On this machine, ITSC fault simulations can be done on two levels: 2.5% (equivalent to 10.2 turns) and 5% (equivalent to 20.4 turns). The DFIM2 characteristics are given in Table 9. Figure 6 to Figure 8 present theoretical and experimental results.

Experimental setup is shown in Figure 5 and includes DFIM2 machine, current sensors, data acquisition system (DAQ), and computer. The sampling frequency of experimental data is $fs = 1$ kHz.

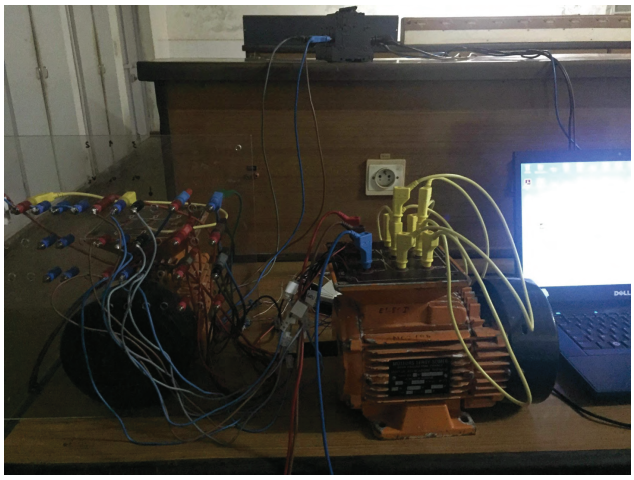

Figure 5. Experimental setup DFIM2.

Table 9. Characteristics of DFIM2.

Specifications	Values	Units
Rated frequency, f	50	Hz
Rated voltage	230/400	V
Rated power, P_n	0.25	kW
Nominal speed	1480	r/min
Rated current	1.8/1	A
Self inductances, l_{sp}, l_{rp}	0.65/0.65	H
Moment of inertia	0.024	kg·m^2
Resistances, r_s, r_r	14.84/8.8	Ω
Number of pole pairs, p	2	

5.2. Experimental Results of DFIM2

In order to illustrate the following comparisons of currents in direct quadrature, the currents will be presented on two cases: theoretical and experimental ones (Figures 6, 7, and 8).

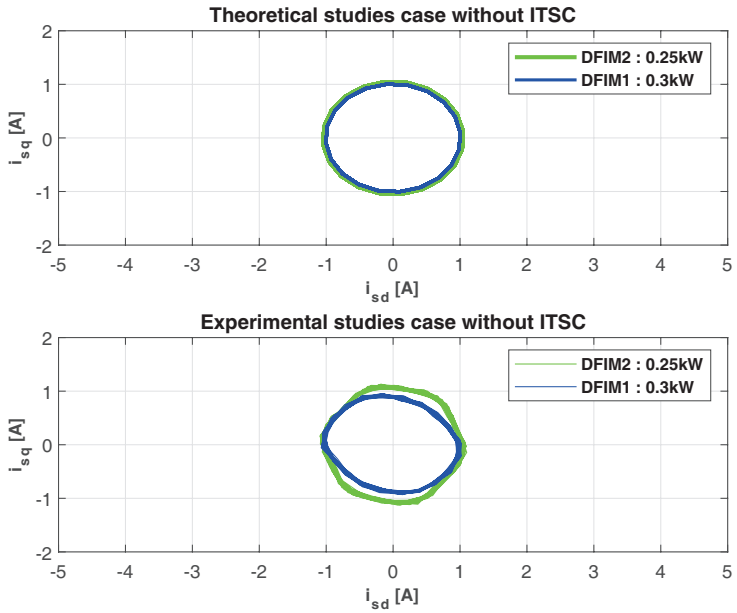

Figure 6. Stator currents in squaring without fault.

In healthy case (Figure 6), it can be seen that Park current representation is very similar on simulations and measurements. The same observation can be made in cases of the 2.5% and 5% ITSC rates (see Figure 7 and Figure 8). On the curves obtained from measurements, those corresponding to DFIM2 are clearly more noised than those of DFIM1: this is because DFIM2 is older than DFIM1 which is new. Nevertheless, the different curves are very similar and show the relevance of the method which focuses only on the detection of ITSC.

As the case of DFIM1 (Table 10), the calculation of the THD_i of i_{sd} and i_{sq} for DFIM1 and DFIM2 is given in Table 3. The THD_i on the two currents i_{sd} and i_{sq} are quite different for the two machines because on the one hand, the measurements were carried out on two different electrical networks (Madagascar for DFIM2 and Corsica for DFIM1), and on the other hand, the DFIM2 is older than the DFIM1.

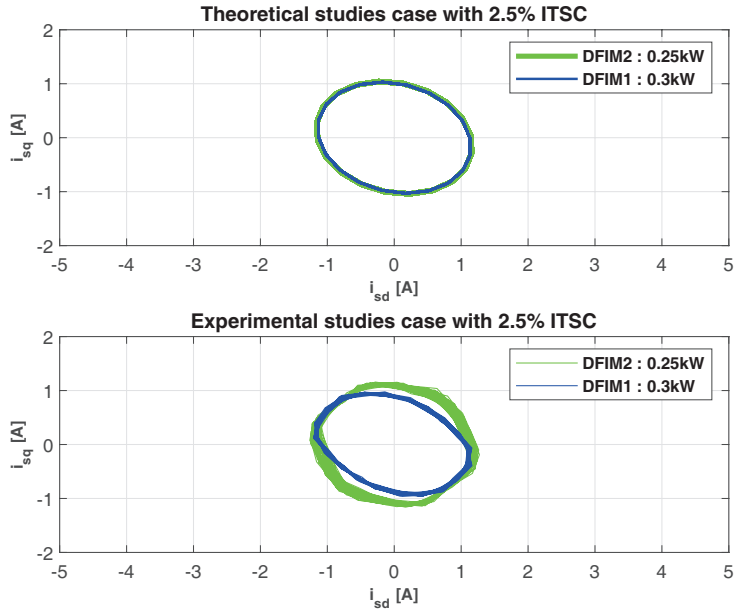

Figure 7. Stator currents in squaring: estimated at 2.5% ITSC.

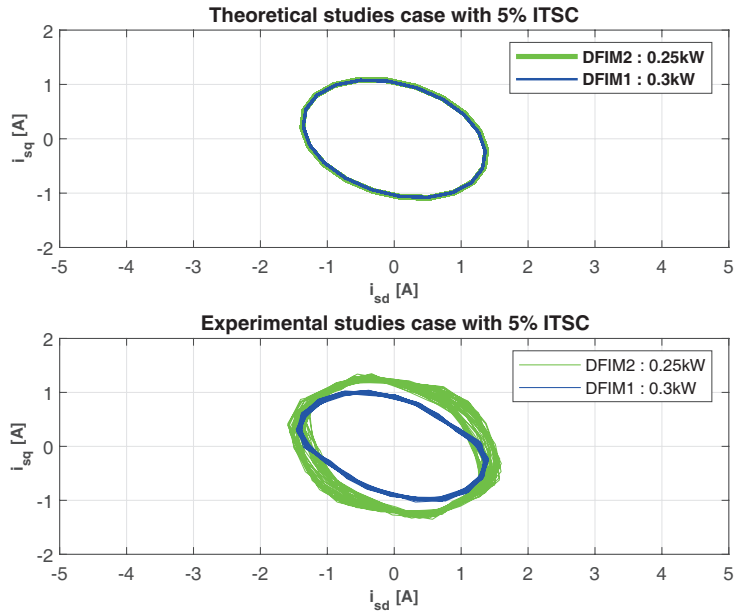

Figure 8. Stator currents in squaring: estimated at 5% ITSC.

After presenting Table 10 and Figure 6 to Figure 8, Table 11 presents the three ellipse parameters: A_{Ex2}, A_{Th2}, A_{Es}, A_{Ex1}, B_{Ex2}, B_{Th2}, B_{Es}, B_{Ex1}, and Phi_{Ex2}, Phi_{Th2}, Phi_{Es}, Phi_{Ex1}. These parameters are obtained from experimental values, theoretical values, and estimated values given by Eqs. (11) to (13). The last column recalls the experimental results obtained for the DFIM1.

5.3. Discussion

The detection of ITSC is not sensitive to the noises coming from bearings, machine age, and electrical network as shown in Table 11. In this table, the ITSC rate can be deduced from major axis A with a

Table 10. THD_i of the two currents i_{sd} and i_{sq} of the DFIM2.

Park currents	**Healthy**	**2.5% ITSC**	**5% ITSC**
i_{sd} (DFIM2)	4.50%	4.73%	6.85%
i_{sq} (DFIM2)	2.68%	2.82%	4.43%
i_{sd} (DFIM1)	4.35%	4.56%	6.78%
i_{sq} (DFIM1)	2.50%	2.70%	4.32%

Table 11. A, B and Phi obtained for the DFIM2.

ITSC rate (%)	$\mathbf{A_{Ex2}}$	$\mathbf{A_{Th2}}$	$\mathbf{A_{Es}}$	$\mathbf{A_{Ex1}}$
n_{sc}	Experimental for DFIM2	Theoretical for DFIM2	Estimation	Experimental for DFIM1
2.5	1.22	1.21	1.23	1.20
5	1.53	1.51	1.55	1.47
ITSC rate (%)	$\mathbf{B_{Ex2}}$	$\mathbf{B_{Th2}}$	$\mathbf{B_{Es}}$	$\mathbf{B_{Ex1}}$
n_{sc}	Experimental for DFIM2	Theoretical for DFIM2	Estimation	Experimental for DFIM1
2.5	1.11	1.12	0.84	0.83
5	1.16	1.15	0.85	0.84
ITSC rate (%)	$\mathbf{Phi_{Ex2}}$	$\mathbf{Phi_{Th2}}$	$\mathbf{Phi_{Es}}$	$\mathbf{Phi_{Ex1}}$
n_{sc}	Experimental for DFIM2	Theoretical for DFIM2	Estimation	Experimental for DFIM1
2.5	0.55 rad	0.52 rad	0.50 rad	0.50 rad
5	0.47 rad	0.45 rad	0.44 rad	0.44 rad

good accuracy. However, the minor axis B and the Phi orientation give lower accuracy. One of the most significant results is the possibility to use the identification obtained from DFIM1 (see Equation (11)) for the second machine with the A parameter corresponding to the major axis. It is very important because,it is now possible to identify ITSC rate using Equation (11) because this one is independent of the studied machine.

This part details the results obtained for each of the three ellipse parameters on the second and third columns of Table 11. These parameters permit to detect and quantify ITSC rate (Table 12), with the three relations given previously in Eqs. (11) to (13). However, the fourth and fifth columns of Table 11 represent A, B, and Phi values obtained from (11) to (13) for DFIM2 and DFIM1, respectively. The total number of DFIM2 turns without ITSC on one phase of the stator winding is 408. Therefore, to facilitate the study, the numbers of shorted turns are presented in Table 13 to compare the accuracy of the different approaches.

Thus, Table 12 illustrates the detection of ITSC rates of DFIM2 from Eqs. (11) to (13) in experimental case, column 2, and theoretical case, column 3. According to experimental major axis A curve obtained with DFIM1, ITSC rate of DFIM1 (columns 2 and 3 of Table 12) can be deduced with good accuracy. However, the two parameters B and Phi cannot be exploited because the obtained results (column 2 and 3 of Table 12) are too far from the ITSC rate taken into account. Table 13 shows the accuracy of the ITSC rate and the corresponding number of shorted turns.

Table 13 contains four distinct columns. The first shows the number of turns without short circuit for DFIM2. Then, the second represents the number of shorted turns and the corresponding ITSC rates. As shown in Table 13: 2.5% of short circuited turns corresponds to 10.2 turns in short circuit. Similarly for the case of 5%, the number of turns in short circuit is equal to 20.4. The third column represents the values of the number of shorted turns and the rates of shorted turns obtained from the three coefficients of the DFIM2 ellipse (A_{Ex2}, B_{Ex2}, and Phi_{Ex2}). Thus, on the two cases: 2.46% and 4.87% of short-circuited turns, there is 2% of error with respect to the representation of the second column of Table 13. An error of 2% corresponds to about 0.2 turns. Finally, the fourth column presents calculations of errors for each approach used in the detection and quantification of ITSC rate. Thus,

Table 12. Detection of the ITSC rate from the ellipses of the DFIM2.

A	p_1 and p_2 experimental data	p_1 and p_2 theoretical data
$\mathbf{A_{Ex2}} = 1.22$	$n_{sc} = 2.46\%$	$n_{sc} = 3.17\%$
$\mathbf{A_{Es}} = 1.23$	$n_{sc} = 2.5\%$	$n_{sc} = 3.25\%$
$\mathbf{A_{Ex2}} = 1.53$	$n_{sc} = 4.87\%$	$n_{sc} = 5.75\%$
$\mathbf{A_{Es}} = 1.55$	$n_{sc} = 5\%$	$n_{sc} = 5.92\%$
B	p_3 and p_4 experimental data	p_3 and p_4 theoretical data
$\mathbf{B_{Ex2}} = 1.11$	$n_{sc} = 48.33\%$	$n_{sc} = 28.33\%$
$\mathbf{B_{Es}} = 0.84$	$n_{sc} = 2.5\%$	$n_{sc} = 0\%$
$\mathbf{B_{Ex2}} = 1.16$	$n_{sc} = 56.67\%$	$n_{sc} = 36.67\%$
$\mathbf{B_{Es}} = 0.85$	$n_{sc} = 5\%$	$n_{sc} = 0\%$
Phi [rad]	p_5 and p_6 experimental data	p_5 and p_6 theoretical data
$\mathbf{Phi_{Ex2}} = 0.55$	$n_{sc} = 0.59\%$	$n_{sc} = 3.74\%$
$\mathbf{Phi_{Es}} = 0.50$	$n_{sc} = 2.5\%$	$n_{sc} = 6.29\%$
$\mathbf{Phi_{Ex2}} = 0.47$	$n_{sc} = 3.58\%$	$n_{sc} = 7.80\%$
$\mathbf{Phi_{Es}} = 0.44$	$n_{sc} = 5\%$	$n_{sc} = 9.52\%$

Table 13. Quantification of the number of turns and associated accuracy.

N_s	N_{scEs}	N_{scEx}	*Accuracy*
408 turns	n_{sc} from $\mathbf{A_{Es}}$	n_{sc} from $\mathbf{A_{Ex2}}$	
	$2.5\% \Leftrightarrow 10.2$	$2.46\% \Leftrightarrow 10.0$	2%
	$5\% \Leftrightarrow 20.4$	$4.87\% \Leftrightarrow 20.0$	2%
	n_{sc} from $\mathbf{B_{Es}}$	n_{sc} from $\mathbf{B_{Ex2}}$	
	$2.5\% \Leftrightarrow 10.2$	$48.33\% \Leftrightarrow 197.2$	1800%
	$5\% \Leftrightarrow 20.4$	$56.67\% \Leftrightarrow 231.2$	1000%
	n_{sc} from $\mathbf{Phi_{Es}}$	n_{sc} from $\mathbf{Phi_{Ex2}}$	
	$2.5\% \Leftrightarrow 10.2$	$0.59\% \Leftrightarrow 2.4$	76%
	$5\% \Leftrightarrow 20.4$	$3.58\% \Leftrightarrow 14.6$	28%

the last column shows the interest of **A** parameter approach because the error made is lower than 2%.

Now that the proposed approach shows its effectiveness with the same power level machines, the next section relates its application to a higher power level machine.

6. DFIM3 STUDY

6.1. DFIM3 Presentation

The DFIM3 has a power range about 30 times higher than DFIM1. The stator of the machine has 48 stator slots, 32 rotor slots, and the number of turns is equal to 252. Nominal values are summarized in Table 14. As in DFIM2 case, the deal is to detect ITSC rate on DFIM3 from the elliptical parameter A (major axis) of the DFIM1.

Table 14. Characteristics of DFIM3.

Specifications	Values	Units
Rated frequency, f	50	Hz
Rated voltage	230/400	V
Rated power, P_n	11	kW
Nominal speed	1425	r/min
Rated current	23/11.32	A
Self inductances, l_{sp}, l_{rp}	0.16/0.16	H
Moment of inertia	0.1	kg·m^2
Resistances, r_s, r_r	1.2/0.8	Ω
Number of pole pairs, p	2	

6.2. Theoretical Results of DFIM3 Study

DFIM3 currents are simulated by Eqs. (1) to (3), and the direct quadrature currents are calculated using Eq. (9). Figure 9 represents the ellipses for ITSC rates of 2.5% and 5%. Figure 10 corresponds to ITSC rates of 10% and 20%. As our laboratory does not have a test bench for higher power level machines, and consider the performance of the theoretical approach compared to the experimental measurements, a purely theoretical study of an 11 kW machine is proposed to observe the robustness of the proposed approach.

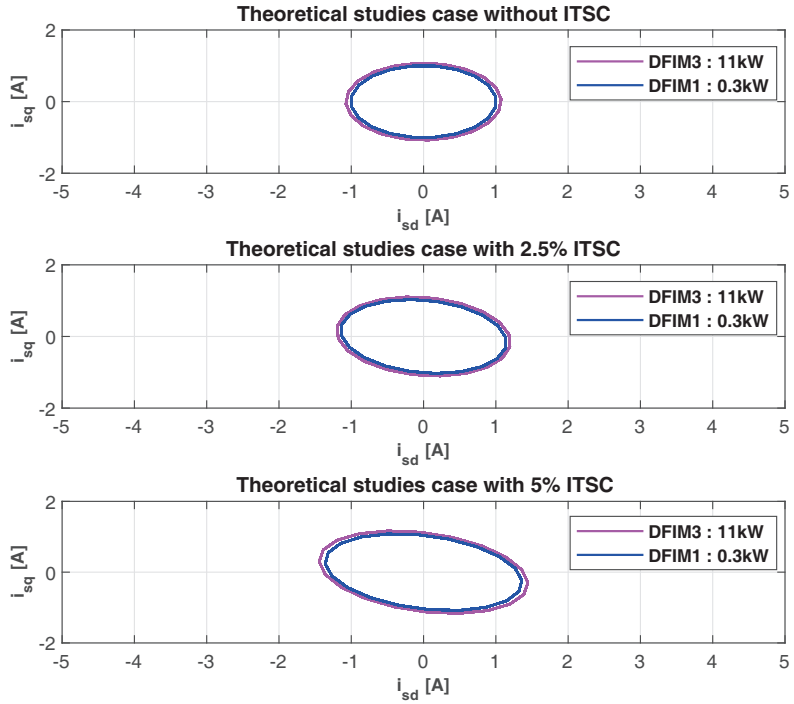

Figure 9. Stator currents in squaring without defect and with defect (estimated at 2.5% and 5% ITSC).

The ellipses from the two machines DFIM1 and DFIM3 are quite similar when the ITSC is less than 5% but quite different when it is greater than 10%. The ellipses in Figure 9 and Figure 10 show that it is possible to consider ITSC detection as well as calculation of the ITSC rate of DFIM3 from DFIM1 data. Table 15 and Table 16 summarize the obtained results for ITSC rates.

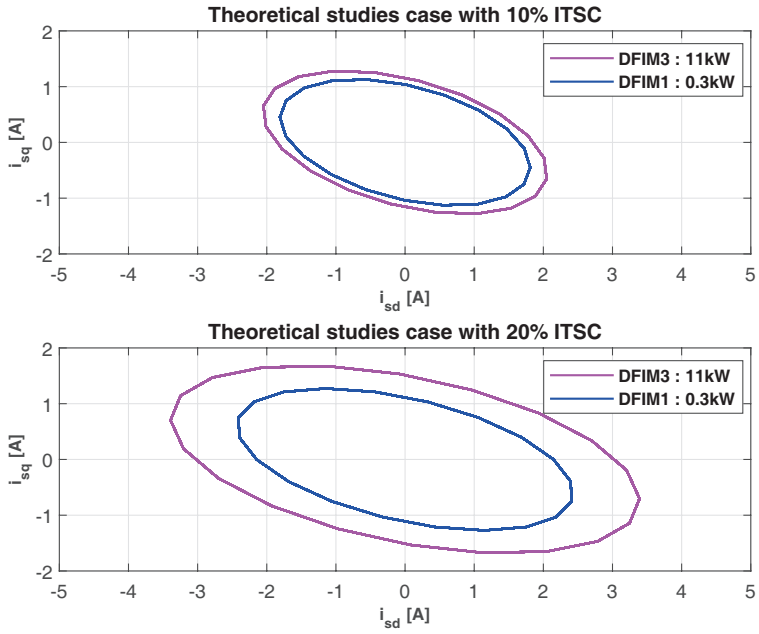

Figure 10. Stator currents in squaring with defect: estimated at 10% and 20% ITSC.

Table 15. *A* obtained for DFIM3.

ITSC rate (%) n_{sc}	$\mathbf{A_{Th3}}$ Theoretical for DFIM3	$\mathbf{A_{Es}}$ Estimate	$\mathbf{A_{Ex1}}$ Experimental for DFIM1
2.5	1.22	1.23	1.20
5	1.55	1.55	1.47
10	2.13	2.22	1.84
20	3.48	3.5	2.57

Table 16. *B* and *Phi* obtained for DFIM3.

ITSC rate (%) n_{sc}	$\mathbf{B_{Th3}}$ Theoretical for DFIM3	$\mathbf{B_{Es}}$ Estimate	$\mathbf{B_{Ex1}}$ Experimental for DFIM1
2.5	1.07	0.84	0.83
5	1.09	0.85	0.84
10	1.18	0.88	0.89
20	1.47	0.94	0.96
ITSC rate (%) n_{sc}	$\mathbf{Phi_{Th3}}$ Theoretical for DFIM3	$\mathbf{Phi_{Es}}$ Estimate	$\mathbf{Phi_{Ex1}}$ Experimental for DFIM1
2.5	0.5 rad	0.50 rad	0.50 rad
5	0.50 rad	0.44 rad	0.44 rad
10	0.40 rad	0.36 rad	0.33 rad
20	0.26 rad	0.26 rad	0.24 rad

6.3. Discussion

After Figure 9 and Figure 10 are presented, Table 15 presents the three ellipse parameters: A_{Th3}, A_{Es}, A_{Ex1}, B_{Th3}, B_{Es}, B_{Ex1} and Phi_{Th3}, Phi_{Es}, Phi_{Ex1}. These parameters are obtained from theoretical and estimated values given by Eqs. (11) to (13). As mentioned in the previous paragraph, the results obtained from parameter A are better than those obtained from parameters B and Phi. This is why the results are published in two separate Tables 15 and 16.

The last column recalls DFIM1 experimental results. The values of the coefficient A_{Th3} presented in Table 15 is close to the parameter A_{Ex1} of the DFIM1 ellipses and the one estimated A_{Es} from Eq. (11). Therefore, the parameter A will allow to quantify the short circuit with accuracy (Tables 17 and 18).

The last column recalls DFIM1 experimental results. The values of the two coefficients B and Phi presented in Table 16 are close to the parameters B_{Ex1} and Phi_{Ex1} of the DFIM1 ellipses and those estimated B_{Es} and Phi_{Es} from Eqs. (12) to (13).

Nevertheless, the results of previous studies (DFM1 and DFM2) have shown that the parameters B and Phi did not permit to deduce short-circuit rate with good accuracy. That is why in the following, only the study of the parameter A will be discussed.

Table 17 summarizes ITSC rates from this parameter A. Table 17 gives ITSC rate obtained from Eq. (11) and DFIM1 data. The results are similar in experimental and theoretical cases.

Table 17. Detection of ITSC rate from A and DFIM1 data.

A	p_1 and p_2 experimental data	p_1 and p_2 theoretical data
$\mathbf{A_{Th3}} = 1.22$	$n_{sc} = 2.46\%$	$n_{sc} = 3.17\%$
$\mathbf{A_{Es}} = 1.23$	$n_{sc} = 2.5\%$	$n_{sc} = 3.25\%$
$\mathbf{A_{Th3}} = 1.55$	$n_{sc} = 5\%$	$n_{sc} = 5.92\%$
$\mathbf{A_{Es}} = 1.55$	$n_{sc} = 5\%$	$n_{sc} = 5.92\%$
$\mathbf{A_{Th3}} = 2.13$	$n_{sc} = 9.46\%$	$n_{sc} = 10.75\%$
$\mathbf{A_{Es}} = 2.22$	$n_{sc} = 10\%$	$n_{sc} = 11.5\%$
$\mathbf{A_{Th3}} = 3.48$	$n_{sc} = 19.47\%$	$n_{sc} = 22\%$
$\mathbf{A_{Es}} = 3.5$	$n_{sc} = 20\%$	$n_{sc} = 22.17\%$

Table 18 specifies the number of shorted turns and the associated accuracy. The number of shorted turns is calculated according to total number of turns. Table 18 shows that detection of the number of turns in short circuit is done with an accuracy lower than 5%, which corresponds to one turn. The result is therefore conclusive.

Table 18. Number of turns short circuited and associated accuracy.

N_s	N_{scEs}	N_{scTh3}	*Accuracy*
252 turns	n_{sc} from $\mathbf{A_{Es}}$	n_{sc} from $\mathbf{A_{Th3}}$	
	$2.5\% \Leftrightarrow 6.3$	$2.46\% \Leftrightarrow 6.2$	2%
	$5\% \Leftrightarrow 12.6$	$4.96\% \Leftrightarrow 12.5$	1%
	$10\% \Leftrightarrow 25.2$	$9.46\% \Leftrightarrow 24$	5%
	$20\% \Leftrightarrow 50.4$	$19.47\% \Leftrightarrow 49.1$	3%

7. CONCLUSION

This article presents a study to detect short-circuit faults between turns, based on the Park transform. The diagnosis makes full use of the geometric shape of the currents in the D-Q basis. Indeed, these currents take the shape of an ellipse which changes according to the severity of the fault. When the number of short-circuited turns increases (2% to 40%), the value of the significant axis grows, and its orientation shifts. This observation permits to develop a methodology to detect this defect. It is therefore possible to quantify the number of short-circuited turns in DFIM windings with excellent accuracy. This approach has been validated with several machines of different power levels. Due to its performance, the developed approach could find a major contribution to short circuit detection. Similarly, it can be useful for ITSC detection on generators installed in wind farms.

ACKNOWLEDGMENT

This work has been partially funded by the CNRS Energy unit (Cellule Energie) through the RESINTER project.

REFERENCES

1. Joksimovic, G. M. and J. Penman, "The detection of inter-turn short circuits in the stator windings of operating motors," *IEEE Transactions on Industrial Electronics*, Vol. 47, No. 5, 1078–1084, 2000, https://doi.org/10.1109/41.873216.
2. Thorsen, O. and M. Dalva, "Condition monitoring methods, failure identification and analysis for high voltage motors in petrochemical industry," *Proceedings of Eighth International Conference on Electrical Machines and Drives*, No. 444, 109–113, Cambridge, UK, September 1997, https://doi.org/10.1049/cp:19971048.
3. El Bouchikhi, E. H., V. Choqueuse, and M. Benbouzid, "Induction machine faults detection using stator current parametric spectral estimation," *Mechanical Systems and Signal Processing*, Vol. 52–53, 447–464, 2015, https://doi.org/10.1016/j.ymssp.2014.06.015.
4. Bonnett, A. H. and C. Yung, "Increased efficiency versus increased reliability," *IEEE Industry Applications Magazine*, Vol. 14, No. 1, 29–36, 2008, https://doi.org/10.1109/MIA.2007.909802.
5. Xu, Z., et al., "Data-driven inter-turn short circuit fault detection in induction machines," *IEEE Access*, Vol. 5, 25055–25068, 2017, https://doi.org/10.1109/ACCESS.2017.2764474.
6. Bonnett, A. H. and G. C. Soukup, "Cause and analysis of stator and rotor failures in three-phase squirrel-cage induction motors," *IEEE Transactions on Industry Applications*, Vol. 28, No. 4 921–937, 1992, https://doi.org/10.1109/28.148460.
7. Lu, Q., T. Breikin, and H. Wang, "Modelling and fault diagnosis of stator inter-turn short circuit in doubly fed induction generators," *IFAC Proceedings*, Vol. 44 No. 1, 1013–1018, 2011, https://doi.org/10.3182/20110828-6-IT-1002.02217.
8. Abdelmadjid, G., B. S. Mohamed, T. Mohamed, S. Ahmed, and M. Youcef, "An improved stator winding fault tolerance architecture for vector control of induction motor: Theory and experiment," *Electric Power Systems Research*, Vol. 104, 129–137, 2013, https://doi.org/10.1016/j.epsr.2013.06.023.
9. Kato, T., K. Inoue, and K. Yoshida, "Diagnosis of stator-winding-turn faults of induction motor by direct detection of negative sequence currents," *Electrical Engineering in Japan*, Vol. 186, No. 3, 75–84, 2014, https://doi.org/10.1002/eej.22350.
10. Im, S. H. and B. G. Gu, "Study of induction motor inter-turn fault part II: Online model-based fault diagnosis method," *Energies*, Vol. 15, No. 3, 977, 2022, https://doi.org/10.3390/en15030977.
11. Roshanfekr, R. and A. Jalilian, "Analysis of rotor and stator winding inter-turn faults in wrim using simulated mec model and experimental results," *Electric Power Systems Research*, Vol. 119, 418–424, 2015, https://doi.org/10.1016/j.epsr.2014.10.018.

12. Razafimahefa, T. D., H. Bilal, N. Heraud, and E. J. R. Sambatra, "Experimental and analytical approaches for investigating low-level inter-turn winding faults in induction machine," *Proceedings of 4th Conference on Control and Fault Tolerant Systems (SysTol)*, 135–140, Casablanca, Moroco, September 2019, https://doi.org/10.1109/SYSTOL.2019.8864786.
13. Bilal, H., N. Heraud, and E. J. R. Sambatra, "Detection of inter-turn short-circuit on a doubly fed induction machine with d-q axis representation," *Proceedings IEEE 61th International Scientific Conference on Power and Electrical Engineering of Riga Technical University (RTUCON), Riga, Latvia, November 2020*, 1–4, https://doi.org/10.1109/RTUCON51174.2020.9316591.
14. Wang, L., Y. Li, and J. Li, "Diagnosis of inter-turn short circuit of synchronous generator rotor winding based on volterra kernel identification," *Energies*, Vol. 11, No. 10, 2018, https://doi.org/10.3390/en11102524.
15. Pires, V. F., T. G. Amaral, and J. F. Martins, "Stator winding fault diagnosis in induction motors using the dq current trajectory mass center," *Proceedings of 35th Annual Conference of IEEE Industrial Electronics*, 1322–1326, Porto, Portugal, November 2009, https://doi.org/10.1109/IECON.2009.5414714.
16. Foito, D., J. Maia, V. Fernão Pires, and J. F. Martins, "Fault diagnosis in six-phase induction motor using a current trajectory mass center," *Measurement*, Vol. 51, 164–173, 2014, https://doi.org/10.1016/j.measurement.2014.02.004.
17. El Hachemi Benbouzid, M., "A review of induction motors signature analysis as a medium for faults detection," *IEEE Transactions on Industrial Electronics*, Vol. 47, No. 5, 984–993, 2000, https://doi.org/10.1109/41.873206.
18. Marques Cardoso, A. J., S. M. A. Cruz, and D. S. B. Fonseca, "Inter-turn stator winding fault diagnosis in threephase induction motors, by park's vector approach," *IEEE Transactions on Energy Conversion*, Vol. 14, No. 3, 595–598, 1999, https://doi.org/10.1109/60.790920.
19. Douglas, H., P. Pillay, and P. Barendse, "The detection of interturn stator faults in doubly-fed induction generators," *Proceedings of Fourtieth IAS Annual Meeting. Conference Record of the 2005 Industry Applications Conference*, Vol. 2, 1097–1102, Hong Kong, China, October 2005, https://doi.org/10.1109/IAS.2005.1518493.
20. Cruz, S. M. A. and A. J. M. Cardoso, "Stator winding fault diagnosis in three-phase synchronous and asynchronous motors, by the extended park's vector approach," *IEEE Transactions on Industry Applications*, Vol. 37, No. 5, 1227–1233, 2001, https://doi.org/10.1109/28.952496.
21. Acosta, G. G., C. J. Verucchi, and E. R. Gelso, "Acurrent monitoring system for diagnosing electrical failures in induction motors," *Mechanical Systems and Signal Processing*, Vol. 20, No. 4, 953–965, 2006, https://doi.org/https://doi.org/10.1016/j.ymssp.2004.10.001.
22. Bilal, H., N. Heraud, and E. J. R. Sambatra, "An experimental approach for detection and quantification of short-circuit on a doubly fed induction machine (DFIM) windings," *J. Control Autom Electr. Syst.*, 1123–1130, Vol. 32, https://doi.org/10.1007/s40313-021-00733-w.